Turkish Journal of Chemistry

http://journals.tubitak.gov.tr/chem/

Research Article

Turk J Chem
(2014) 38: 297 – 308

doi:10.3906/kim-1303-32

Optimization of $LiFePO_4$ synthesis by hydrothermal method

Muhsin MAZMAN[1,*], Ömür ÇUHADAR[2], Davut UZUN[1], Ercan AVCI[1], Emre BİÇER[1], Tevhit Cem KAYPMAZ[1], Ümit KADİROĞLU[2]

[1]TÜBİTAK Marmara Research Center Energy Institute, Gebze, Kocaeli, Turkey

[2]Department of Chemistry, Faculty of Arts and Sciences, Kocaeli University, Kocaeli, Turkey

Received: 12.03.2013 • **Accepted:** 19.09.2013 • **Published Online:** 14.03.2014 • **Printed:** 11.04.2014

Abstract: Optimization of the $LiFePO_4$ cathode active material synthesis process in the hydrothermal method consists of many factors, including pH, carbon coating, particle size optimization, sintering and hydrothermal synthesis temperature. The main goal of this study is to determine the effect of particle size, pH and carbon coating on capacity and cycle performance. In this study, $LiFePO_4$ cathode active materials were prepared at different pH (6.5 and 8.5) and temperature (160 and 180 °C) levels using the hydrothermal method. The hydrothermal synthesis products were sintered at 400, 500, 600, and 700 °C with 5% and 7% carbon source. The initial discharge capacity was observed as 130 mAh g^{-1} for the sample that was sintered at 700 °C. However, a 14% capacity loss was measured after 100 cycles. Additionally, the sample was ground for 10 h in a ball mill and sintered at 700 °C. The capacity was then increased to 151 mAh g^{-1} and the capacity loss was measured as 7% (140 mAh g^{-1}) after 200 cycles.

Key words: $LiFePO_4$, Li-ion, battery, cathode, carbon coating

1. Introduction

$LiFePO_4$ batteries have become a focus of research, especially for electric vehicle applications, owing to the fact that they are cheap and relatively safe. They also have a high theoretical capacity of 170 mAh g^{-1}, good cycle life, and the ability to sustain high current density. However, the advantages of $LiFePO_4$ are still open to research because of the low electronic conductivity of $LiFePO_4$ and its delithiated form $FePO_4$, as well as the low ionic conductivity of these phases.[1,2]

Electronic conductivity may be improved by metal doping and carbon coating,[3–6] and low ionic conductivity may be improved through reduction of particle size. Previous studies showed that particle sizes differed with respect to the synthesis method and the synthesis medium (pH, pressure, etc.).[7] One of the most relevant methods for reducing particle size was reported to be the hydrothermal method by Aimable et al., who investigated supercritical water medium in hydrothermal synthesis to reduce impurities, particle size, and cost.[2]

Lithium iron phosphate may be produced through methods of solid state synthesis, mechanical- or spray-drying, sol-gel, and hydrothermal synthesis. Hydrothermal synthesis was shown to be useful in obtaining small-sized fine particles.[8,9] Lithium iron phosphate cathode material was first synthesized at high temperatures; however, in an effort to reduce costs and energy usage it was demonstrated in 2001 that hydrothermal synthesis can indeed be used to synthesize lithium iron phosphate at the low temperature of 120 °C, which made

*Correspondence: muhsin.mazman@tubitak.gov.tr

hydrothermal synthesis a favorable option. It was shown that $LiFePO_4$ is resistant to chemical oxidation and reduction. Approximately 7% of the irregular iron atoms constitute an electron concentration on the lithium side.[10]

The most important point in $LiFePO_4$ synthesis is capturing the correct phase. Once that goal is achieved, there are several basic procedures available to increase capacity and performance, such as carbon coating, sintering, adding atoms to the structure, reducing particle size (down to nanometer scale), altering particle structure, changing the pH value, and varying the different parameters (solvent, reaction temperature, and solution concentration).[10]

Carbon coating is one of the basic methods used to improve the weak electrical conductivity of electrode material and to increase the performance thereof. In order to increase conductivity, sometimes coating materials other than carbon are used, as well. In this work, carbon coating will remain the main process to be used. In addition to improving conductivity, carbon coating also serves as a dispersant among the particles.[4] Carbon coating may be applied by adding organic or polymer compounds within the frame of synthesis, as well as by adding organics such as sugar or ascorbic acid during the sintering phase after the synthesis.[11] The effects of the carbon residual on the $LiFePO_4$ are essential to electrochemical performance.[12] Increased sp^2 hybrid character carbon coating has been observed to increase conductivity compared to that of sp^3 character. Carbon coating may affect the formation of nanostructure particles and high specific surfaces.[3] The pore sizes on the coating surface may be controlled by selecting proper parameters for the synthesis. In addition, the thermal separation of carbon compounds is a complex process. Breaking of the covalent bonds, rebonding of the carbon chains and structure, and properties of the carbon are determined by the conditions of the synthesis.[4]

Another parameter affecting capacity is the pH of the hydrothermal synthesis. Although lithium iron phosphate synthesis takes place within the pH interval of 5–11, there have been investigations to determine the best possible interval. Liu et al. reported on the effect of pH value on synthesis. Their work revealed that the Li ratio of the structure changes for various pH values. It was reported that the highest Li involvement occurred around pH 8.[13]

The synthesis temperature is yet another matter affecting the synthesis. The synthesis temperature for hydrothermal synthesis of $LiFePO_4$ must exceed 120 °C. In syntheses at lower temperatures, Li/Fe disorder is observed. This phenomenon causes limited lithium insertion and removal in the structure because of the tunnel blockage by iron, which leads to a loss in capacity. In order to obtain olivine structures without interference, a minimum synthesis temperature of 175 °C is required.[11]

This study focuses on the effects of pH, synthesis temperature, sintering temperature, and carbon ratio on $LiFePO_4$ capacity. Carbon contents after the hydrothermal synthesis at different pH values and sintering temperatures were determined to optimize the carbon additive requirement in different conditions.

2. Results and discussion

The hydrothermal synthesis products were sintered at 400, 500, and 600 °C. The best capacity results were measured from sample 2, which was prepared at pH 8.5, 180 °C hydrothermal synthesis temperature, and 600 °C sintering temperature. The capacities are shown in Figure 1 for 3 samples (samples 1, 2, and 3). As shown in Figure 1, 400 and 500 °C were not enough to sinter $LiFePO_4$. Increasing the temperature to 600 °C had a positive effect on the capacity. However, we noticed that temperatures higher than 600 °C would yield better sintering results. Thus, sample 2 was handled and sintered at 700 °C.

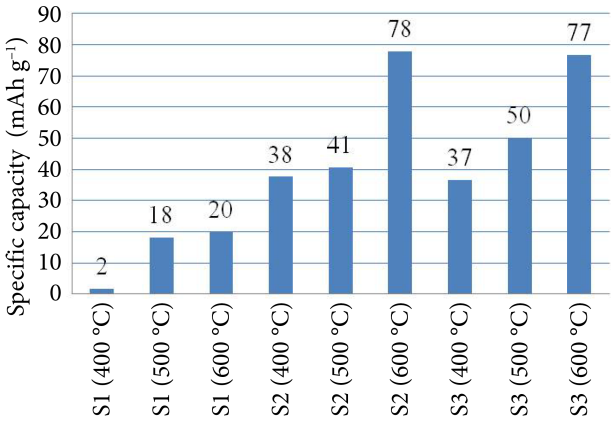

Figure 1. Capacity values for S1, S2, and S3 at 400, 500, and 600 °C sintering temperatures.

As far as we know, another significant effect on capacity is that of carbon coating. While evaluating capacity, coated carbon contents on the material should be taken into account. To determine this effect, carbon contents of the materials were measured by elemental analyses and the results are given in Table 1. As shown in Table 1, carbon rates were affected by sintering temperatures and pH values. For these initial materials at a lower pH (6.5), carbon rate was measured as 4.39% at 600 °C. The sucrose added to prevent Fe^{+2} oxidation during the hydrothermal process was enough for carbon coating and there was no need for a carbon source in the annealing process. On the other hand, at pH 8.5 the carbon rates dropped below 1% and the annealing process needed carbon source additives for carbon coating. Sucrose, which was added to prevent the oxidation of Fe^{2+} in the hydrothermal synthesis, forms levulinic acid at lower pH values.[14] This causes a decrease of pH in the reaction media for sample 1 (S1) of 6.5 to 4.2, for sample 2 (S2) of 8.5 to 5.6, for sample 3 (S3) of 8.5 to 5.3, and finally for sample 4 (S4) of 8.5 to 7.2. As seen here, the pH value of S1 (initial pH of 6.5) was decreased to pH 4.2. It is well known that sucrose constitutes carbon in acidic media in the process of hydrothermal carbonization.[15,16] Therefore, the carbon ratio of S1 was measured higher than that of other samples prepared at pH 8.5.

Table 1. Carbon rates (%) at different sintering temperatures.

	Carbon content (%)		
Sample	400 °C	500 °C	600 °C
1	4.77	4.94	4.39
2	1.32	1.13	1.04
3	1.31	1.14	0.69

Electrochemical test results show that sintering temperatures should be optimized to enhance electrochemical performance and capacity. As shown in Figure 1 for S2, electrochemical performance and capacity of the materials were increased by increasing the temperature and carbon coating thickness in the sintering process. The first results showed that the study could focus on enhancement of storage capacity for S2 by optimizing the sintering temperature and carbon coating thickness.

Therefore, S4 was synthesized mirroring the conditions of S2 and split into 3 parts, 1 of which was prepared without carbon additive (S4.1), while the other 2 were prepared with 5% (S4.2) and 7.5% (S4.3) carbon source additive (sucrose), respectively. These 3 parts were sintered at 700 °C and then tested as cathode material. After the sintering process, carbon content was measured as 0.8% for S4.1. This much carbon was caused by

carbonization of the sucrose additive. However, when the initial carbon additive was taken as 5%, the resulting carbon rate was measured as 3.2% following the sintering process for S4.2. Similarly, for S4.3, the initial carbon additive was 7.5%, with the final carbon rate dropping to 4.5%.

Figure 2 shows the cyclic voltammetry (CV), impedance, and capacity results for S4 derivatives S4.1, S4.2, and S4.3. The capacities were measured as 70 mAh g^{-1}, 130 mAh g^{-1}, and 98 mAh g^{-1} for S4.1, S4.2, and S4.3, respectively. However, in the impedance results, the sample with the 3% carbon content showed the highest capacity performance, since the increasing carbon rate decreased the impedance of the material. Within the obtained electrochemical results, the optimal carbon content was found to be around 3%. In order to obtain this rate after sintering, the initial carbon source addition should be 5%.

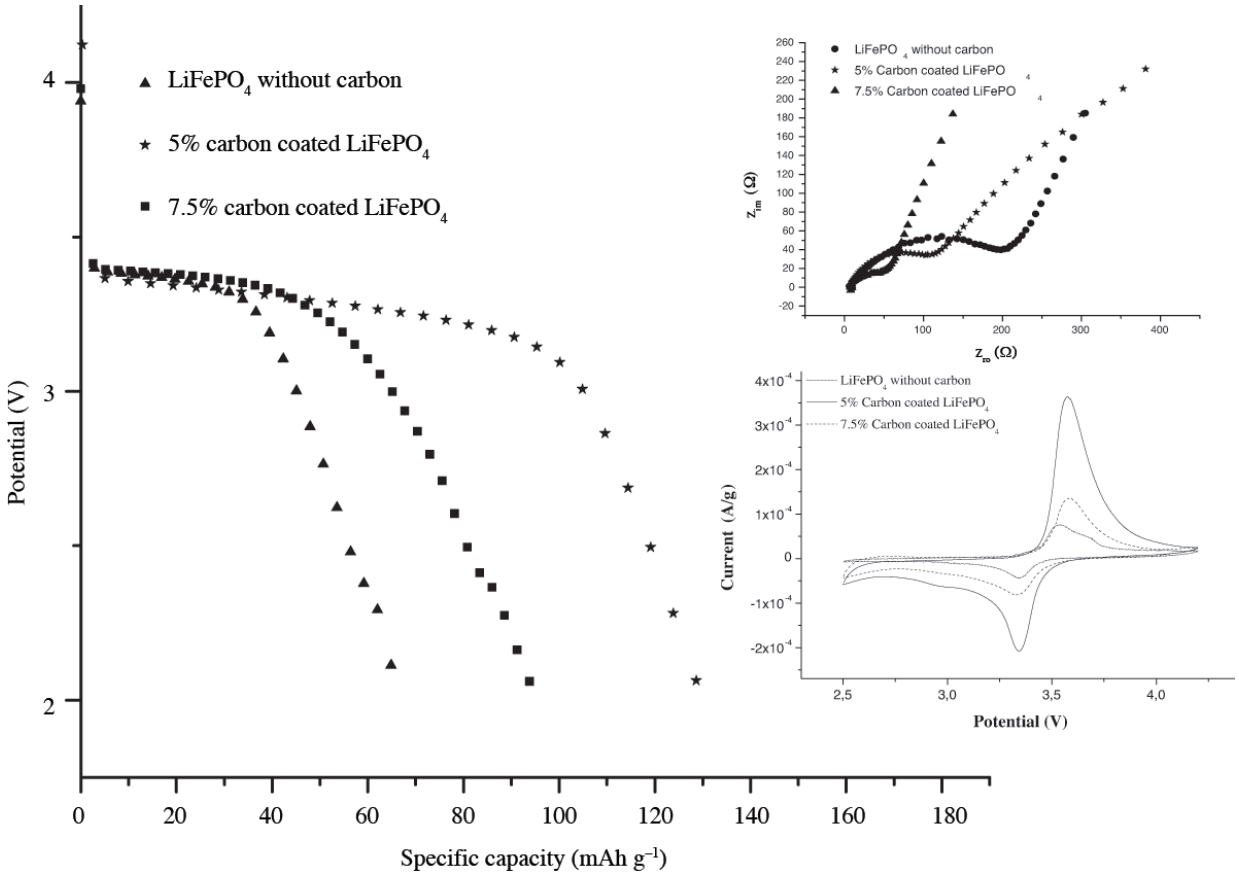

Figure 2. Capacity, impedance (between 1 MHz and 0.5 Hz), and CV (between 2.5 and 4.2 V) values for samples that were prepared with 0%, 5%, and 7.5% carbon coating.

For the characterization of the samples, X-ray diffraction (XRD) results for S2 at different temperatures (400, 500, 600, and 700 °C) are shown in Figure 3. The comparison of XRD patterns revealed that all samples were in the same phase and that the results matched with standard orthorhombic $LiFePO_4$ values.[17] As seen in Figure 3, the samples had impurities at the temperatures of 400, 500, and 600 °C, which gradually disappeared as the temperature increased to 700 °C, whereupon the capacity values also increased. The impurities were due to the reduction of Fe in $LiFePO_4$ and the formation of iron compounds such as Fe_2P and Fe_2O_3.[18,19]

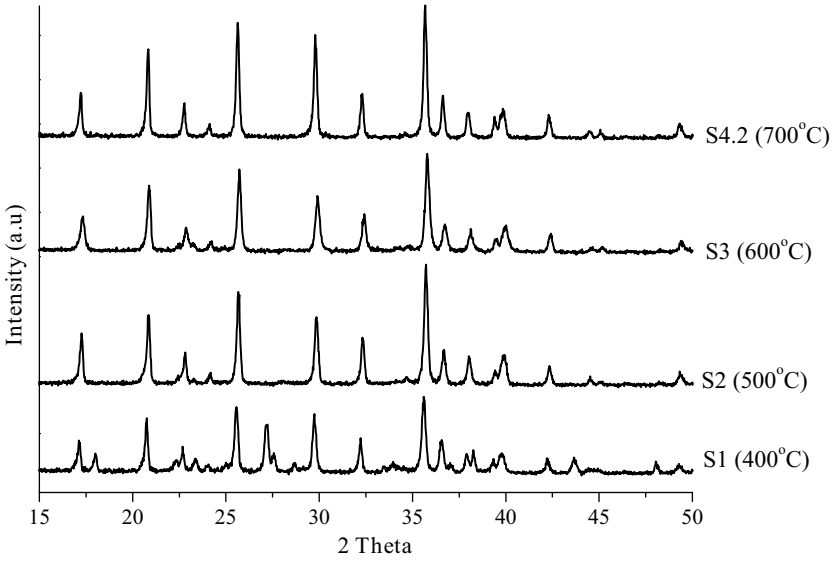

Figure 3. XRD results for S1, S2, S3, and S4.2 (scan rate: 2 °C min^{-1}).

Fourier transform infrared (FTIR) spectra indicated the olivine structure of the samples. As shown in Figure 4, the peaks of FTIR spectra of samples are within the 400–1600 cm^{-1} range. The peak distribution is within the ranges of 460–675 cm^{-1} and 950–1160 cm^{-1}. The sharp peaks at around 635 cm^{-1}, 945 cm^{-1}, and 1135 cm^{-1} show the symmetric vibrations of P-O bands. The peaks centered at 1075 cm^{-1} can be attributed to intramolecular asymmetric vibrations of P-O. The peaks at 463 and 501 cm^{-1} are symmetric bending vibrations of O-P-O and at around 540 cm^{-1} is the asymmetric vibration of O-P-O bands. The bands at 590 cm^{-1} and 635 cm^{-1} are assigned to molecular symmetric vibrations of Fe-O bands.[20] As a result, samples sintered at 500, 600, and 700 °C are in the olivine phase of $LiFePO_4$ and the sample contains other phosphate anions, as indicated by the weak peak around 910 cm^{-1}.

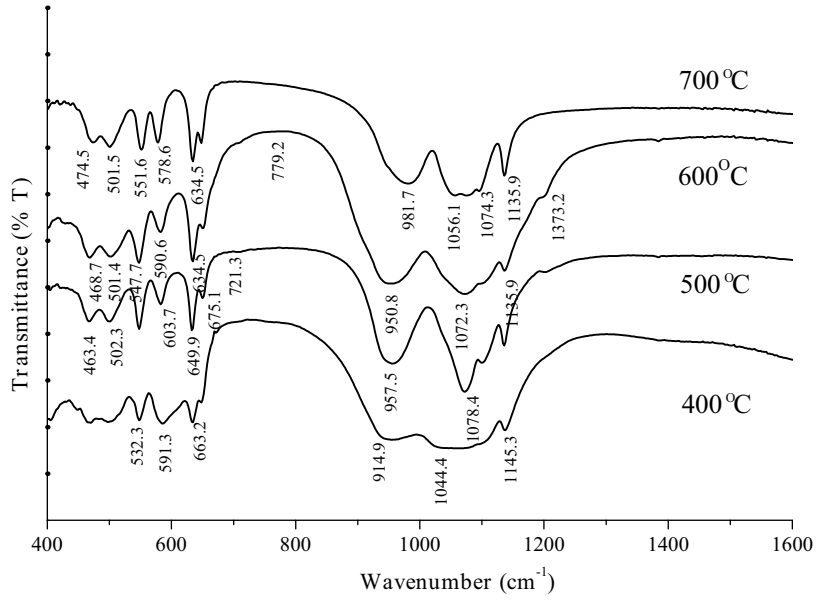

Figure 4. FTIR results for S1, S2, S3, and S4.2.

The highest electrochemical results were obtained for S4.2. Therefore, the studies were focused on determining the cycle performance of the S4.2. A 100 charge/discharge cycle sequence was conducted at the following C rates: 0.1 C (5 cycles), 0.3 C (5 cycles), 0.5 C (5 cycles), 1 C (40 cycles), 2 C (40 cycles), and finally again 0.1 C (5 cycles). In the first 5 cycles at 0.1 C, a capacity of 130 mAh g^{-1} was observed, whereas it dropped to 95 mAh g^{-1} at 0.3 C, 85 mAh g^{-1} at 0.5 C, 75 mAh g^{-1} at 1 C, 60 mAh g^{-1} at 2 C, and 110 mAh g^{-1} at 0.1 C. As shown in Figure 5, the capacity decreased with the increasing C rate. After 100 cycles, a capacity loss of 14% was calculated for 0.1 C.

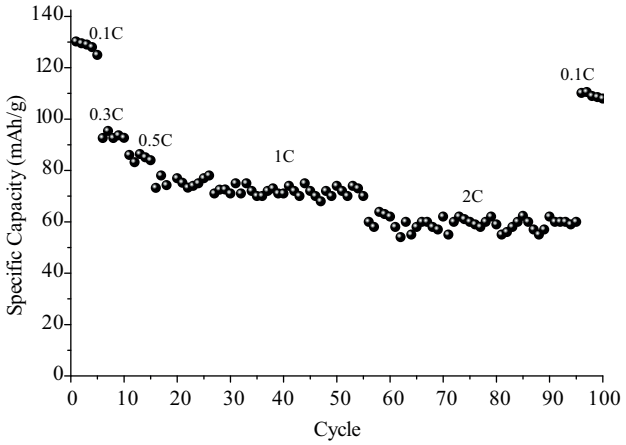

Figure 5. Cycle performance for S4.2 at different C rates.

These results led us to investigate the effects of the particle size, shape, and carbon coating of the materials on capacity. After the hydrothermal synthesis, 1 part of S4 was ground for 10 h in a ball mill (S4.4) to decrease the particle size mechanically. Figures 6a and 6b depict the particle size analysis of the samples. The percentage of particle size distribution is given in Table 2. As shown in Figure 6a, at 400 °C the particles were spread in a wide range, with similar spreads for 500 and 600 °C. At 700 °C, smaller particles were formed. On the other hand, Figure 6b shows that the particle size decreased because of the carbon content and that the smallest particles were produced by mechanical grinding. Scanning electron microscope (SEM) images show the particle size distribution, as shown in Figures 7a and 7b for S4.1 (annealing at 700 °C without carbon) and Figures 7c and 7d for S4.4 (after milling, annealed at 700 °C with 5% carbon). As shown in Figure 7, particle sizes were decreased and the distribution became more homogeneous as a result of the milling and carbon coating processes.

Table 2. Particle size distribution of the samples.

	d(0.1) μm	d(0.5) μm	d(0.9) μm	Specific surface area (m^2 g^{-1})
S1 (400 °C without carbon)	1.999	5.711	17.152	1.4
S2 (500 °C without carbon)	4.218	9.779	18.561	0.8
S3 (600 °C without carbon)	4.150	9.792	18.669	0.805
S4.1. (700 °C without carbon)	1.832	4.195	9.364	1.73
S4.2. (5% carbon additive)	0.119	2.897	47.196	15
S4.3. (7.5% carbon additive)	0.114	2.793	52.565	15.8
S4.4. (5% carbon additive with milling)	0.098	0.546	25.665	22.8

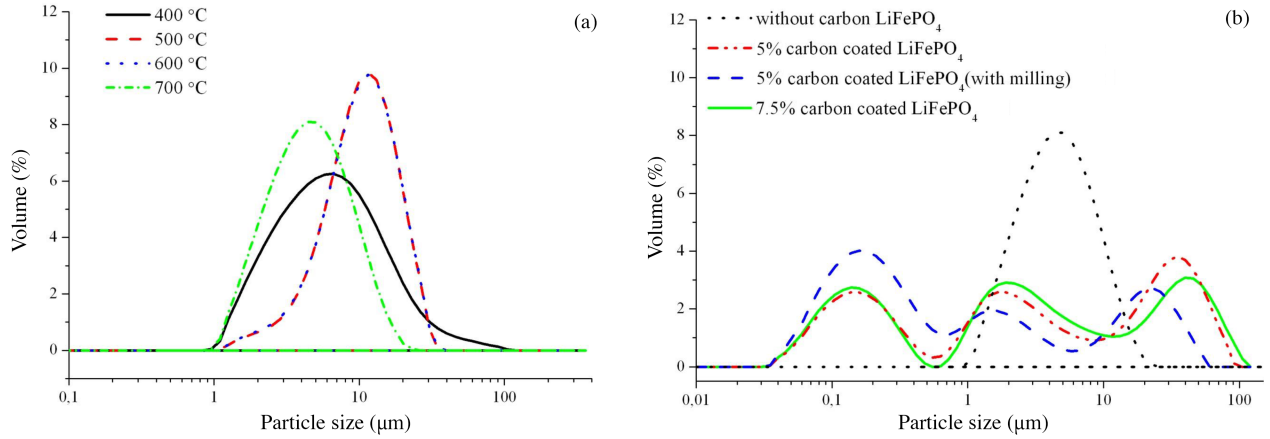

Figure 6. a) Particle size distribution at different sintering temperatures, b) effect of carbon ingredients and mechanical grinding on particle size distribution.

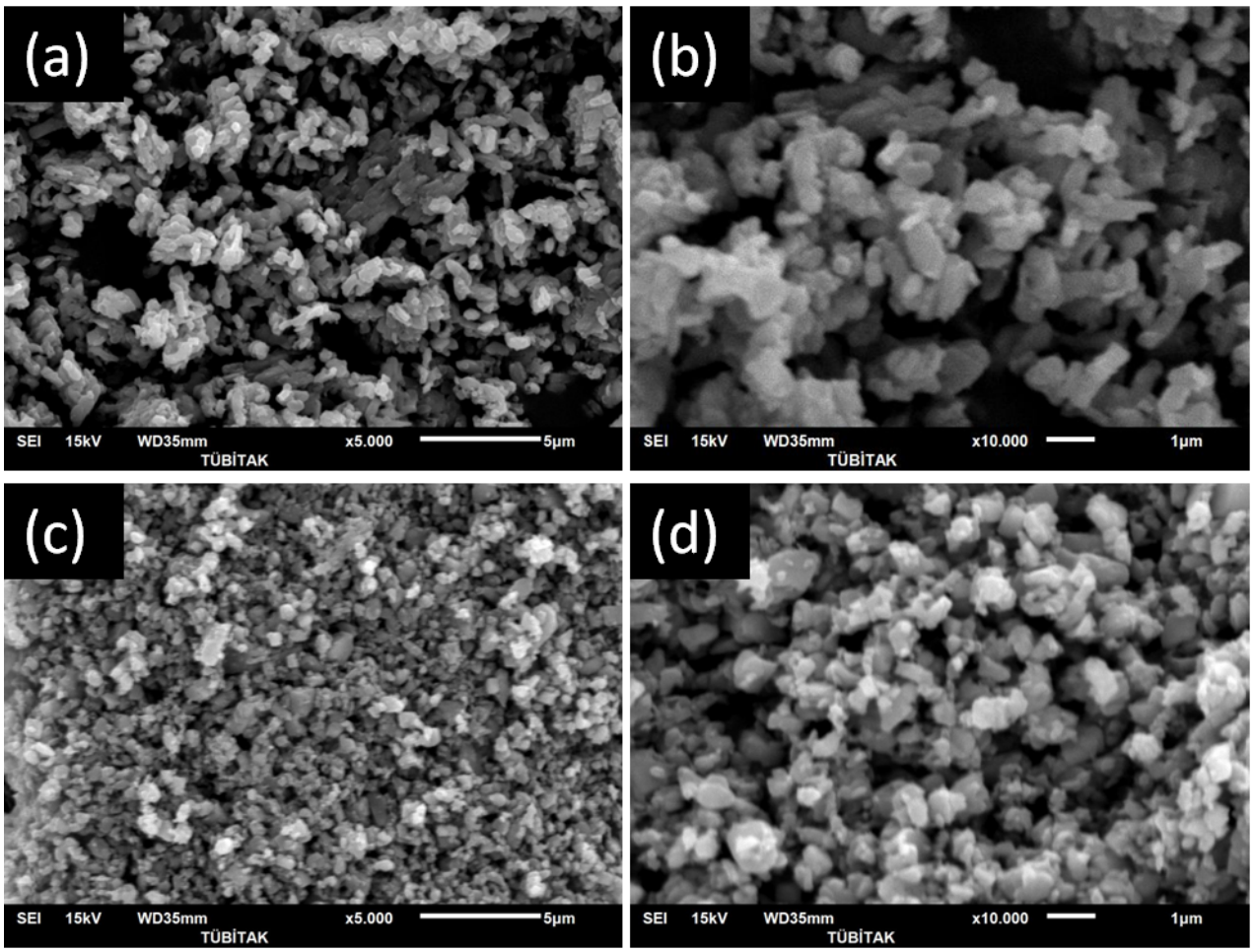

Figure 7. SEM images for S4.1, which was prepared without additional carbon, at 5 μm (a) and at 1 μm (b), and for S4.4, which was prepared with 5% additional carbon source, at 5 μm (c) and at 1 μm (d).

The capacity of sample S4.4 was measured as 151 mAh g^{-1} at 0.1 C. Additionally, 200 charge/discharge cycle sequences were conducted at the following C rates for S4.4: 0.1 C (10 cycles), 0.3 C (10 cycles), 0.5 C (10 cycles), 1 C (100 cycles), 2 C (50 cycles), 5 C (10 cycles), and finally again 0.1 C (10 cycles). Thereafter, in the first 10 cycles at 0.1 C, a capacity of 150 mAh g^{-1} was observed, with the following results for the other measurement points: 128 mAh g^{-1} at 0.3 C, 98 mAh g^{-1} at 0.5 C, 98 mAh g^{-1} at 1 C, 87 mAh g^{-1} at 2 C, 80 mAh g^{-1} at 5 C, and 140 mAh g^{-1} at 0.1 C. As shown in Figure 8, the capacity at higher C rates yielded better results compared to other samples. The capacity loss for 0.1 C was calculated as 7% after 200 cycles.

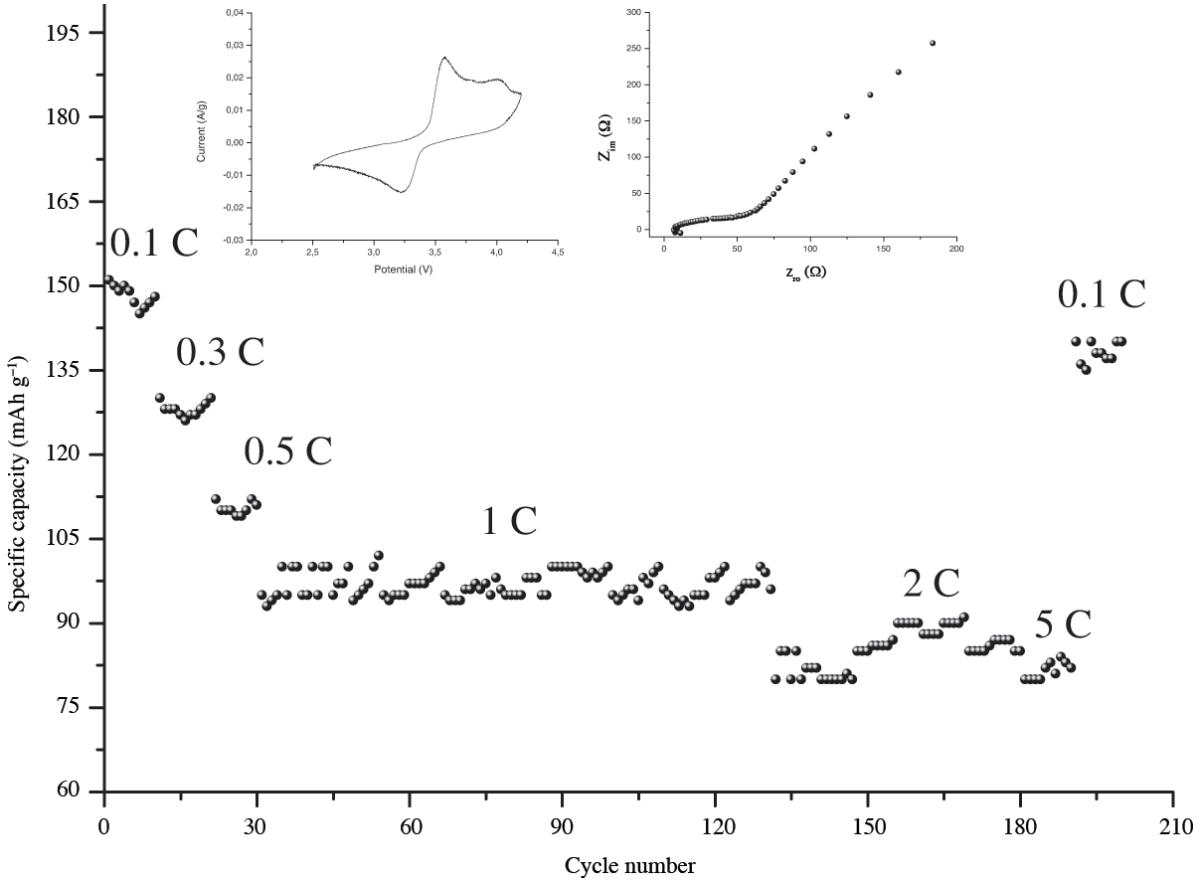

Figure 8. Impedance (between 1 MHz and 0.5 Hz), CV (between 2.5 and 4.2 V), and cycle performance for S4.4 at different C rates.

As shown here, the size of the particles had an effect on capacity loss. The other significant effects were the carbon rate and the coating thickness. Figure 9 shows the carbon coating effect (S4.1, S4.2, S4.3, S4.4) measured by transmission electron microscope (TEM). A quick survey of Figures 9a and 9b shows that the shapes of the particles were spherical for S4.1 and that no carbon coating was observed around them. S4.1 was prepared without any additional carbon source present during the sintering process. In Figures 9c and 9d, it is shown that the spherical shape changed and a nonuniform carbon coating occurred around the particle with a thickness varying between 10 and 30 nm for S4.2. S4.2 was prepared with a 5% carbon source additive. The aforementioned nonuniformity caused a capacity loss by decreasing electronic conductivity.[21] This effect can be suppressed by decreasing particle sizes to nanoscale. Figures 9e and 9f display the results obtained for S4.3,

which was prepared with a 7.5% carbon source additive. As shown in Figure 9f, carbon coating was uniform and had a thickness of around 40 nm. S4.3 has a lower capacity than S4.2 due to the thicker coating. On the other hand, S4.4, which was prepared by milling S4.2, had the lowest coating distance, as shown in Figures 9g and 9h. S4.4 had the highest capacities at 0.1 C, as well as at other C rates.

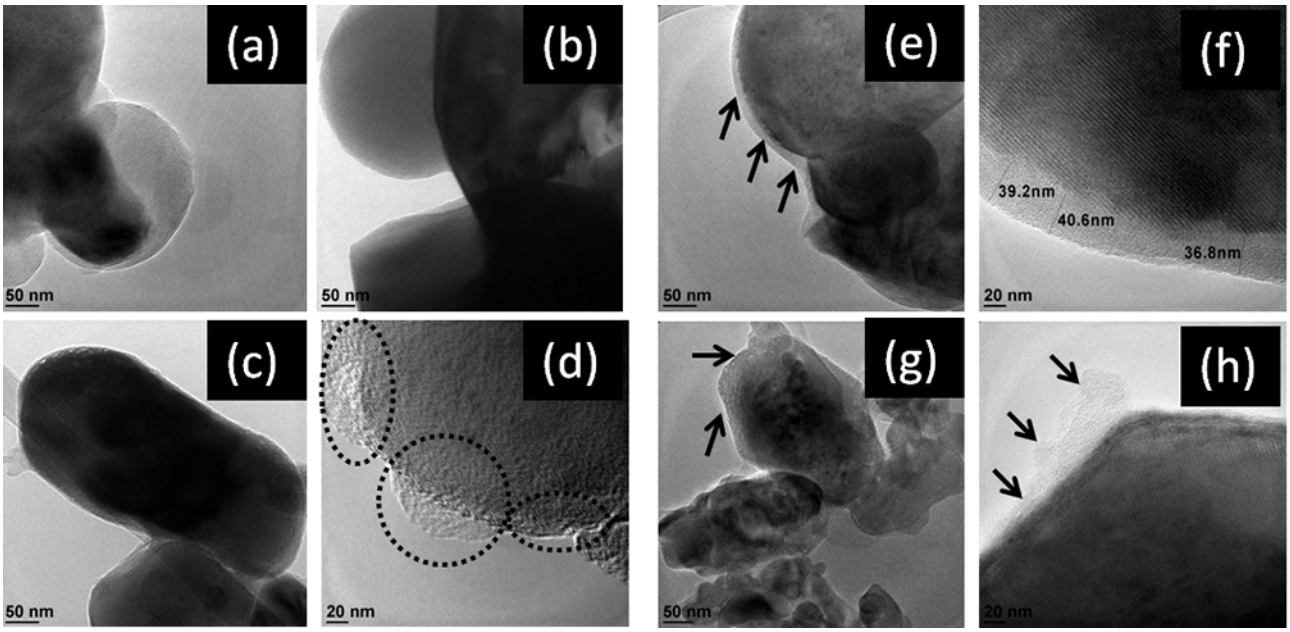

Figure 9. TEM images for S4.1, which was prepared without additional carbon (a and b); for S4.2, which was prepared with 5% additional carbon source (c and d); for S4.3, which was prepared with 7.5% additional carbon source (e and f); and S4.4, which was prepared by milling and with 5% additional carbon source (g and h).

To summarize, olivine structured $LiFePO_4$ samples were prepared using the hydrothermal method at different pH values, temperatures, and carbon content. Initial materials chosen were $FeCl_2.4H_2O$, $NH_4H_2PO_4$, and $LiNO_3$. The results showed that selecting a base pH value of around 8.5 had a favorable effect on capacity. The hydrothermal synthesis should also be performed at around 180 °C to obtain a proper olivine structure. Additionally, sucrose ($C_{12}H_{22}O_{11}$) additive had a positive effect on suppressing Fe^{+3}, dependent on temperature. Thus, the final carbon content decreased to below 1% with ascending temperature in the sintering process. Higher performance among all samples was observed for those with 3% carbon content. Therefore, it was concluded that an optimized cathode active material should contain around 3% carbon, with sucrose containing 5% carbon, as an additive. Additionally, it was noted that higher or lower values of carbon content had a negative effect on capacity. The highest capacity for the initial materials was obtained when the pH was maintained at 8.5 during the synthesis, with 3% carbon content, a synthesis temperature of 180 °C, and a sintering temperature of 700 °C. The mechanical milling before the sintering process was found to increase capacity to 151 mAh g^{-1}. The capacity increase and C rate capability depend on particle size and carbon coating; those with nanoscale particles and thin carbon coatings (around 10 nm) exhibited higher capacity. At the same time, decreasing the particle size to nanoscale also reduced the carbon coating thickness. Consequently, it is reported in the literature that by using different additives as a coating source, the capacities could increase to 164 mAh g^{-1}.[22,23]

3. Experimental

$LiFePO_4$ was prepared using the hydrothermal method from the initial materials of $FeCl_2.4H_2O$ (99%, ABCR), $NH_4H_2PO_4$ (98%, Carlo Erba), $LiNO_3$ ($\geq$98%, Merck), and sucrose ($C_{12}H_{22}O_{11}$, Carlo Erba) in the molar ratio of Li:Fe:P = 3:1:1. Sucrose was added as a reducing agent for prohibiting the conversion of Fe^{+2} to Fe^{+3} during the hydrothermal reaction.[11] Sucrose was added to act as the carbon source in carbon coating while preventing the generation of α-Fe_2O_3 during the annealing process. All the initial materials were solved in minimum solvent (water) and mixed. The final pH value was measured as 3.5, which was adjusted by the addition of NH_3. The solution was then transferred to a hydrothermal synthesis tank. The synthesis was achieved under argon atmosphere at 30 atm pressure, 120 rpm mixing speed, and 6 h waiting time. Synthesis conditions are given in Table 3.

Table 3. Synthesis conditions of the samples.

Samples	pH	Hydrothermal synthesis temperature (°C)	Sintering temperature (°C)
1	6.5	180	400, 500, 600
2	8.5	180	400, 500, 600
3	8.5	160	400, 500, 600
4	8.5	180	700

3.1. Sample preparation

S1, S2, and S3 were prepared by adding the solutions directly and adjusting the conditions to pH 6.5 and synthesis temperature 180 °C for S1, to pH 8.5 and synthesis temperature 180 °C for S2, and to pH 8.5 and synthesis temperature 160 °C for S3. S4 was prepared similar to S2, but the material solutions were added slowly and in sequence.

Hydrothermal synthesis was achieved under an argon atmosphere at 30 atm and 120 rpm for 6 h. After the synthesis, the samples were washed with distilled water and acetone several times and dried at 80 °C in a vacuum for 6 h. Dry samples were ground for 1 h at 150 rpm in a ball mill and annealed in an argon atmosphere furnace at 400, 500, and 600 °C for 6 h. The sintered samples were then milled at 150 rpm for 10 min. S4 was split into 4 parts, which were annealed under 3 different conditions: 1 without carbon source additive and the other 2 with 5% and 7.5% carbon source additives, respectively. One part of S4 was also ground for 10 h in a ball mill and then sintered with 5% carbon additives.

3.2. Cathode preparation

The cathodes were prepared by observing the following rates: active material at 80%, conductive carbon (Super P) at 12%, and PVDF in NMP at 8%. Cathode additives were mixed for 30 min in a ball mill at 150 rpm and 3.5 mg of cathode material was coated on a 1.5 cm^2 aluminum disk. The disks were dried for 2 h at 105 °C in a vacuum and hot pressed at 90 °C and under 500 kg cm^{-2} of pressure. Pressed electrodes were then dried for 2 h at 105 °C in vacuum conditions and used for coin cell (CR2032) preparation against lithium metal anode with 1 M $LiPF_6$ as an electrolyte (w/w 1:1, EC:DEC).

3.3. Characterization

The crystal structures of the materials were characterized with a Shimadzu XRD-6000 using Cu Kα radiation operating at 40 kV and 30 mA in the range of 3–90 °C (2θ) at a scan rate of 2 °C min^{-1}. Thermogravimet-

ric/differential thermal analysis (Mettler TGASDTA851e, in air atmosphere between room temperature and 900 °C with heating rate of 15 °C min^{-1}) and the LECO TruSpec Elemental Analyzer were used to determine the carbon content in the material. FTIR transmittance spectroscopy was recorded with a Shimadzu FTIR 8001 PC Infrared Spectrometer at room temperature in the 400–4000 cm^{-1} range.

Particle size distribution was measured with the Malvern S2000, material shapes were determined by SEM (JEOL JSM-6510LV), and carbon coating was determined by TEM (FEI Technai G^2F20).

3.4. Electrochemical characterization

Electrochemical impedance measurements were recorded with a frequency range between 1 MHz and 0.5 Hz. CV studies were carried out with an EL-Cell 3-electrode electrochemical cell by using lithium as a counter and reference electrode and a prepared electrode as a working electrode. CV curves were performed in the voltage range of 2.5–4.2 V at a scan rate of 0.1 mV s^{-1}. Charge and discharges curves were measured between 2.0–4.2 V at 0.1 C for 3 samples (S1, S2, and S3) and at 0.1 C, 0.3 C, 0.5 C, 1 C, and 2 C for S4. The electrochemical measurements of coin cells were measured by using the Princeton Applied Research VersaSTAT MC analyzer system.

Acknowledgment

This study was supported by the Scientific and Technological Research Council of Turkey (TÜBİTAK, project number 111T567). The authors would also like to thank to Dr Günhan Kaytaz for his valuable contributions in discussions.

References

1. Jugovic, D.; Uskokovic, D. *J. Power Sources* **2009**, *190*, 538–544.
2. Aimable, A.; Aymes, D.; Bernard, F.; Le Cras, F. *Solid State Ionics* **2009**, *180*, 861–866.
3. Yun, N. J.; Ha, H. W.; Jeong, K. H.; Park, H. Y.; Kim, K. *J. Power Sources* **2006**, *160*, 1361–1368.
4. Wang, J.; Sun, X. *Energy Environ. Sci.* **2012**, *5*, 5163–5185.
5. Zhang, Q.; Wang, S.; Zhou, Z.; Ma, G.; Jiang, W.; Guo, X.; Zhao, S. *Solid State Ionics* **2011**, *191*, 40–44.
6. Goktepe, H.; Sahan, H.; Ulgen, A.; Patat, S. *J. Mater. Sci. Technol.* **2011**, *27*, 861–864.
7. Qingzhu, S.; Xiuqin, O.; Li, W.; Guangchuan, L.; Zuorui,W. *Mater. Res. Bull.* **2011**, *46*, 1398–1402.
8. Zhang, Y.; Huo, Q.; Du, P.; Wang, L.; Zhang, A.; Song, Y.; Lv, Y.; Li, G. *Synth. Met.* **2012**, *162*, 1315–1326.
9. Dokko, K.; Koizumi, S.; Sharaishi, K.; Kanamura, K. *J. Power Sources* **2007**, *165*, 656–659.
10. Chen, J.; Whittingham, M. S. *Electrochem. Commun.* **2006**, *8*, 855–858.
11. Chen, J.; Wang, S.; Whittingham, M. S. *J. Power Sources* **2007**, *174*, 442–448.
12. Goktepe, H.; Sahan, H.; Kilic, F.; Patat, S. *Ionics* **2010**, *16*, 203–208.
13. Liu, J.; Jiang, R.; Wang, X.; Huang, T.; Yu, A. *J. Power Sources* **2009**, *194*, 536–540.
14. McKenzie, B. F. *Org. Synth.* **1929**, *9*, 50.
15. Demir-Cakan, R.; Baccile, N.; Antonietti, M.; Titirici, M. M. *Chem. Mater.* **2009**, *21*, 484–490.
16. Demir-Cakan, R.; Makowski, P.; Antonietti, M.; Goettmann, F.; Titirici, M. M. *Catal. Today* **2010**, *150*, 115–118.
17. Shu, H.; Wang, X.; Wu, Q.; Liu, L.; Liang, Q.; Yang, S.; Ju, B.; Yang, X.; Zhang, X.; Wang, Y. et al. *Electrochim. Acta* **2012**, *76*, 120–129.

18. Yun, N. J.; Ha, H. W.; Jeong, K. H.; Park, H. J.; Kim, K. *J. Power Sources* **2006**, *160*, 1361–1368.
19. Qingzhu, S.; Xiuqin, O.; Li, W.; Guangchuan, L.; Zuorui, W. *Mater. Res. Bull.* **2011**, *46*, 1398–1402.
20. Yu, F.; Zhang, J.; Yang, Y.; Song, G. *Electrochim. Acta* **2009**, *54*, 7389–7395.
21. Gaberscek, M.; Dominko, R.; Jamnik, J. *Electrochem. Commun.* **2007**, *9*, 2778–2783.
22. Avci, E.; Mazman, M.; Uzun, D.; Biçer, E.; Şener, T. *J. Power Sources* **2013**, *240*, 328–337.
23. Uzun, D.; Doğrusöz, M.; Mazman, M.; Biçer, E.; Avci, E.; Şener, T.; Kaypmaz, T. C.; Demir-Cakan, R. *Solid State Ionics.* **2013**, *249–250*, 171–176.